Architectural Innovations for Efficient Denoising and Classification: A Manual vs. Neural Architecture Search Comparison

Thomas Markhorst[1,2] Osman Semih Kayhan[1,2] Jan C.van Gemert[2]
[1] Bosch Security Systems [2] Delft University of Technology

Abstract

In this paper, we combine image denoising and classification, aiming to enhance human perception of noisy images captured by edge devices, like security cameras. Since edge devices have little computational power, we also optimize for efficiency by proposing a novel architecture that integrates the two tasks. Additionally, we alter a Neural Architecture Search (NAS) method, which searches for classifiers [16], to search for the integrated model while optimizing for a target latency, classification accuracy, and denoising performance. Our NAS architectures outperform our manually designed alternatives in both denoising and classification, offering a significant improvement to human perception. Moreover, our approach empowers users to construct architectures tailored to domains like medical imaging, surveillance systems, and industrial inspections.

1. Introduction

The intersection of edge devices, such as security cameras, and deep learning has sparked an interest in optimizing neural networks for inference time, further referred to as latency. Common tasks to optimize for such efficiency are object classification and detection, which mainly aid in machine perception. However, when aiming to improve human perception, the quality of the processed image is equally significant. This importance intensifies particularly for images containing noise, which can arise from various sources such as low-light conditions, sensor noise, or any stage within the image processing pipeline. We focus on using an efficient model to enhance the human perception of noisy images.

Domains relying on human image perception but challenged by noisy images, like medical imaging [21], surveillance systems [29], and industrial inspections [8], can benefit from recently proposed denoising Convolutional Neural Networks (CNNs) [12, 41]. As CNNs denoise better than traditional methods [5, 11]. Fast CNN denoisers [10, 42] are required to accommodate the real-time requirement of the affected domains. However, denoisers are not able to remove all noise, which is not always enough for human image perception.

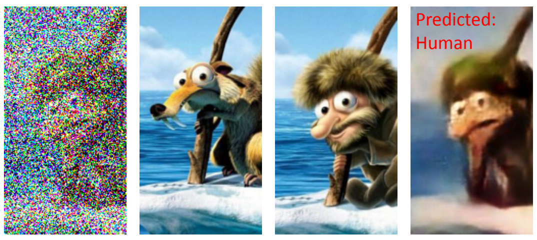

Figure 1. We take a noisy image (a), which can be interpreted as an animal (b) or human (c). DC-NAS S is used to denoise and classify (a), aiming to improve human perception (d). Note, in a real application (b) and (c) would not be available, which increases the difficulty of interpreting the noisy image. Artist: Astkhik Rakimova

We further improve human understanding of the image by combining denoising with machine perception, like image classification. For instance, while improving the quality of a noisy image would assist a security guard, the ability to classify the scene content could help interpret the denoised image. This classification could distinguish between a human and a large animal. Therefore, we investigate models which can leverage the benefits of both denoising and classification to enhance human understanding in real-time.

A model combining both denoising and classification is studied in [17], focusing on denoising performance. In addition, we optimize for efficiency, which is required for edge devices, and classification. Our efficiency definition is based on two elements: (i) latency reduction while (ii) retaining denoising performance and classification accuracy. These elements could be optimized using independent classification and denoising models. However, we propose an architecture combining the tasks more efficiently.

First, we employ established model design approaches to enhance independent denoising and classification models, such as model scaling [20, 31] and the introduction of efficient operators [27]. Although the models are optimized, they still operate separately, resulting in unnecessary overhead. Hence we propose and compare two methods that join both tasks, yielding a novel and efficient architecture.

Adjusting this architecture for each device and desired latency can be laborious and requires expert knowledge. These issues have recently garnered interest, leading to the emergence of new automated architecture search techniques, which have achieved competitive results in image classification [32, 35]. Moreover, recent Neural Architecture Search (NAS) approaches incorporate latency in their loss function, enabling the design of architectures tailored to specific latency requirements. Combining NAS with the proposed architecture provides a seamless and efficient approach to designing denoising and classification models for diverse use cases.

We find that our proposed efficiency-focused architecture consistently outperforms our more straightforward alternative. This is observed for both the manually and NAS designed models. In addition, our NAS models significantly outperform the manually designed ones in denoising and classification performance.

We have the following contributions. (i) We introduce a novel architecture to combine denoising and classification efficiently. The novelty lies in sharing an encoder between the denoiser and the classifier. (ii) We propose modifications to an existing NAS method for classification [16] to stabilize its search, which improves the performance of the found architectures. (iii) We extend an existing NAS method to search for a model which combines denoising and classification, optimized with respect to a target latency, classification accuracy, and denoising performance.

Since no prior work proposes a joint efficient model for denoising and classification, we study the tasks both separately and joint in Section 3. The findings are used as expert knowledge to construct the NAS method in Section 4.

2. Related work

Denoising. Image denoising aims to reconstruct a clean image x from its observed noisy variant y. This relation can be formulated as $y = x + n$, where we assume n to be additive white Gaussian noise (AWGN). Neural network-based denoisers offer faster inference and good performance compared to traditional denoising methods like BM3D [5] and WNNM [11]. The interest in deep learning for denoising started with DnCNN [41], a simple Convolutional Neural Network (CNN). Encoder-decoder architectures became popular due to their efficient hierarchical feature extraction. Specifically, UNet [26] whose skip-connections between the en- and decoder enhance the denoising process as shown in follow-up methods [12, 19, 24]. The interest in the UNet structure continued with transformer architectures [9, 34]. In this paper, our denoisers are based on UNet, ensuring our findings can translate to most related work.

Efficient classification. Optimization for efficiency is generally achieved by either compressing pre-trained networks [23] or designing small networks directly [27, 32]. We focus on efficient design, for which handcrafted models and neural architecture search (NAS) have played essential roles. Studies proposing handcrafted models often introduce efficient operators [14, 27, 43] or scaling methods [31]. These efficient operators are used in NAS methods [32, 35] aiming for the automated design of efficient neural networks. Such an operator is the inverted residual with a linear bottleneck (MBConv) introduced in MobileNetV2 [27]. In our models, we study scaling methods and MBConv's efficiency characteristic.

Neural Architecture Search. The use of reinforcement learning (RL) for neural architecture search introduced efficient architectures with competitive classification performance [13, 25, 30, 32]. However, their discrete search space is computationally expensive. Differentiable NAS (DNAS) methods [1, 18, 35] significantly reduce this cost by relaxing the search space to be continuous using learnable vectors α for selecting candidate operations, which allows for gradient-based optimization. The popularity of DNAS started with DARTS [18], which searches a cell structure. Due to the complex design and repetitiveness throughout the network of the cell structure, follow-up works [16, 35] search operators for every layer instead of constructing repeating cells.

Pitfalls of DNAS are the collapse of search into some fixed operations and a performance drop when converting from the continuous search network to the discretized inference network [4, 38, 39]. TF-NAS [16] addresses these issues with an adaptation in the search algorithm, which lets the search model mimic the discrete behavior of the inference model. In addition, TF-NAS searches an architecture with a target latency by adding a latency loss to the search optimization. Because of these properties, we use TF-NAS as a baseline for our NAS study.

Existing NAS methods for denoising are either not reproducible [22], have a cell-based search space [40], or do not have an encoder-decoder [3] architecture. Instead, we use a layer-based search space and encoder-decoder structure.

Joint classification and denoising. In [36], the positive influence of denoising methods on classification performance is discussed. Moreover, [17] proposed a joint model where a VGG classifier [28] is attached to a denoiser similar to UNet. They report qualitative improvement of the denoised images when adding the classification loss to the denoiser's optimization. Although the model denoises well, the proposed model is not optimized for classification and efficiency, nor is another joining method studied.

3. Gaining expert knowledge on DC-Net

For the separate classification and denoising tasks, we construct a baseline model. Additionally, methods to increase their respective efficiency are studied, resulting in a reduced version of the baseline models. The different sizes of the classifier and denoiser are used to study joining methods and their efficiency.

Dataset & settings. We generate a controlled synthetic data set to study the behavior of the classifier and denoiser when applying model scaling, replacing the convolutional operations, and combining both models. The dataset consists of 30k images, each with a random monotone background in a gray tint [0.1 - 0.3] with two randomly placed non-overlapping MNIST [7] digits. We use two digits to increase the complexity of the denoising task. For experiments including classification, the two digits are extracted from the image using ground truth locations. These extracted digits are separately used as input for the classifier. In the experiments where noise is required, for either denoising or noisy classification, synthetic Gaussian noise is added. This noise is zero mean, and the intensity of the noise is controlled using the standard deviation (σ) of the distribution. Figure 4a shows a sample, and Figure 4b its noisy variant. To test the model behavior on an extensive noise range, every model is trained and tested on eleven σ values evenly spaced on the interval $[0, 1]$.

The models are trained using Adam optimizer with 1E-3 learning rate (LR), plateau LR scheduler, and 100 epochs.

Since the experiments with the controlled data set are not targeted at a specific device, the metric defining efficiency should not depend on a device. Such a metric is computational power, most commonly defined as Floating Point Operations (FLOPs), which we use as the primary metric. Despite being device dependent, we assess latency as a secondary metric. The latency is measured with a batch size of 32, 100 warm-up inference passes and averaged over 1000 inference passes. Denoising performance is quantified using the Peak Signal-to-Noise Ratio (PSNR) and Structural Similarity Index (SSIM) metrics [33]. For both metrics, higher is better.

3.1. Efficient Classification

Experimental setup. Our baseline classifier (Conv-L) consists of two convolutional, one global max pooling, and a linear layer. Each convolutional layer also has a group normalization [37], max pooling, and ReLU activation function.

To construct the reduced version, we use two methods similar to previous works [27, 31]. In the first method, we replace the second convolutional layer with an MBConv layer. Three expansion rates are used $\{1, 2.5, 4\}$: (i) rate 1 is the lowest possible value, (ii) rate 4 matches the number of FLOPs of the baseline, and (iii) rate 2.5 is in the middle of those two. The second reduction method is to lower the number of filters in the baseline, also called the model width. Using these techniques, models with three different FLOP sizes are constructed, $\{$S, M, L$\}$. We use the following naming scheme, Conv-x and MBe-x, where x represents the FLOP size and e is the expansion rate of the MBConv.

Model	Size	Exp. rate	FLOPs (K) $\downarrow$	Lat. (ms) $\downarrow$	Acc (%) $\uparrow$
Conv-L	L	-	447	0.336	63.2
MB1-S	S	1	177	0.300	56.2
MB2.5-M	M	2.5	350	0.384	64.1
MB4-L	L	4	424	0.468	64.9

Table 1. Classification models using convolutions (Conv) and MBConvs (MB), designed for three different FLOP targets: $\{$S, M, L$\}$, to compare scaling methods. MB models scale down more efficiently than normal Conv models.

The models are trained using Cross Entropy loss. We report the accuracy averaged over all 11 noise levels.

Exp. 1: Conv vs MBConv comparison. According to [27], the MBConv layer should be more efficient than a normal convolutional layer. Therefore, when comparing the two operators in our network, we expect the version with an MBConv layer to need fewer FLOPs for the same accuracy. In Table 1, the MB models with expansion rates 2.5 (MB2.5-M) and 4 (MB4-L) classify better than the Conv-L model with fewer FLOPs. However, with an expansion rate of 1 (MB1-S), the accuracy drops 7% compared to Conv-L. Therefore, [27]'s theory also holds for the noisy classifier, but only for the higher expansion rates.

Conclusion. The MBConv layer can replace the convolutional layers. Additional experiments in Appendix A study the scaling method. We find that compared to the Conv models, the MB models also scale down more efficiently by first reducing the expansion rate, possibly followed by a width reduction. Scaling effectively reduces the number of FLOPs.

MB2.5-M has the second-best accuracy with low FLOPs and a latency close to the baseline, Conv-L. Therefore, MB2.5-M is used as the reduced classifier. We also use MB2.5-M as the new baseline classifier as it outperforms the old baseline, Conv-L, in FLOPs and accuracy.

It is important to note that the reduction in FLOPs instantiated by using MBConvs, does not translate to a latency reduction in these experiments. This issue is discussed previously in [32]. Since the target of these experiments is FLOPs and the latency increase is manageable, we place minimal emphasis on the latency.

3.2. Efficient Denoising

Experimental setup. For denoising, the baseline and reduced version are constructed by performing a hyperparameter study on UNet similar to [20]. Figure 2 shows the UNet architecture along with its hyperparameters to tune. We explore the parameters one at a time, starting with the

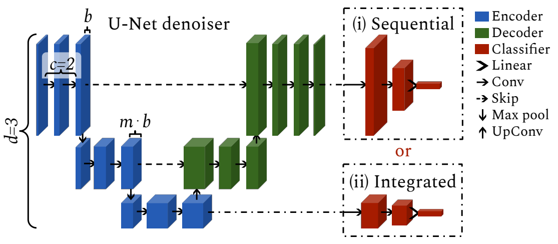

Figure 2. Schematic of the UNet, with hyperparameters base feature map width (b), depth (d), channel multiplier (m) and convolutions per layer (c). For the joint model either attaching the classifier (i) Sequential or (ii) Integrated.

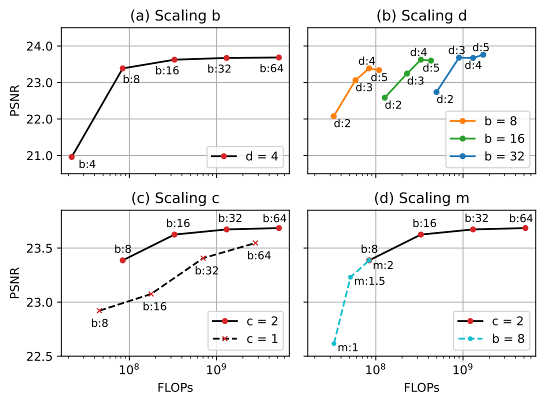

Figure 3. UNet hyperparameter (Figure 2) scaling experiments. Shows how altering a specific hyper-parameter influences denoising performance and FLOPs. We only show PSNR results of σ=0.8, as the other results show the same trend. We find that b and m scale down efficiently, d and c do not.

number of base features maps b, then the UNet depth d, the feature map multiplier m, and the number of convolutional blocks per layer c. In the original UNet: $\{b = 64, d = 5, m = 2, c = 2\}$. Altering these hyperparameters can greatly reduce the model size. Similar to the classification experiments, we also study the ability of the MBConv operator to increase efficiency in the denoiser. The models are trained using Charbonnier loss [2].

Exp. 1: The base feature map width *b*. In this experiment, we aim to find the relevant range of b. Since b is multiplied at every level, the number of feature maps throughout all layers depends on it, which makes it a powerful hyper-parameter. We use $d = 4$ and the other hyper-parameters as in the original UNet, then we test $b \in \{4, 8, 16, 32, 64\}$. The trend in Figure 3.a shows that the performance and FLOPs increase with b. We observe that the trend is significantly disrupted by $b = 4$. Conversely, the performance difference between $b = 32$ and $b = 64$ is small,

Model	FLOPs (M) ↓	Lat. (ms) ↓	Metric	Noise level (σ) 0.2	0.4	0.8	1
UNet Baseline	1301.8	7.10	PSNR ↑	33.9	29.5	23.8	22.3
			SSIM ↑	0.99	0.98	0.95	0.92
UNet Reduced	51.2	2.38	PSNR ↑	33.2	28.7	23.3	22.0
			SSIM ↑	0.99	0.98	0.94	0.92

Table 2. Compares Baseline and Reduced UNet denoisers. The reduced model has significantly lower FLOPs and latency yet similar denoising performance.

but the network size quadrupled. Therefore in further experiments, we focus on $b \in \{8, 16, 32\}$.

Exp. 2: The UNet depth *d*. Given the robustness of b, we are interested in how reducing d compares in terms of efficiency. Figure 3.b displays the performance of the architectures with the selected $b \in \{8, 16, 32\}$ testing $d \in \{2, 3, 4, 5\}$. We observe that reducing d causes a drop in denoising performance, whereas b retains performance better, also in Figure 3.a. Therefore b scales down more efficiently. The models with $d = 3$ or 4 denoise most efficient. Especially for the smaller models, $d = 4$ performs well.

Exp. 3: The number of conv blocks per layer *c*. Does reducing c further increase efficiency? To test this, we take the best-performing settings, $d = 4$ and $b \in \{8, 16, 32, 64\}$, and compare $c = 1$ and $c = 2$. Figure 3.c shows that the model with $c = 2$ outperforms $c = 1$. Therefore reducing c does not benefit the model's efficiency.

Exp. 4: The feature map multiplier *m*. We test if our smallest model could be further reduced in size by lowering m. We take $d = 4$ and $b = 8$, and compare $m \in \{1, 1.5, 2\}$. Figure 3.d shows that the reduction to $m = 1.5$ retains performance. For $m = 1$, the performance drops. Reducing m to 1.5 could therefore be used to scale down the model when further reducing b significantly decreases performance.

Conclusion. To construct the reduced and baseline denoiser, we use the smallest and largest value from the found hyperparameter ranges. Resulting in baseline: $\{b = 32, d = 4, m = 2, c = 2\}$ and reduced: $\{b = 8, d = 4, m = 1.5, c = 2\}$. Table 2 compares the two models for a selection of the noise levels. Although the reduced model has significantly fewer FLOPs and lower latency, the denoising performance is relatively similar to the baseline denoiser.

The UNet hyper-parameter experiments are replicated using MBConvs, which lead to similar findings. Moreover, the Conv UNet slightly outperforms the MB model. Therefore, the Conv model is used.

3.3. Joint model: DC-Net

Experimental setup. We construct a baseline and reduced joint model, Denoising-Classifying Network (DC-Net). The baseline uses MB2.5-M as classifier and the baseline UNet as denoiser. Reduced DC-Net also uses MB2.5-M as classifier but the reduced UNet as denoiser.

DC-Net	Type	FLOPs (M) ↓	Lat. (ms) ↓	PSNR ↑	SSIM ↑	Acc. (%) ↑
Baseline	**Int.**	1301.8	**7.14**	**32.8**	**0.97**	88.1
	Seq.	1302.1	7.55	27.1	0.95	**89.6**
Reduced	**Int.**	51.2	**2.41**	**29.9**	**0.97**	86.2
	Seq.	51.5	2.83	25.2	0.92	**87.6**

Table 3. Compares the reduced and baseline joint models, both the Integrated and Sequential method trained on the synthetic noise dataset. Integrated performs significantly better in denoising and slightly worse in classification. Integrated also scales down better.

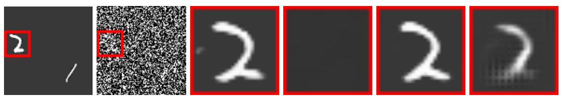

(a) GT (b) σ=0.8 (c) **Int. S** (d) Seq. S (e) **Int. L** (f) Seq. L

Figure 4. Ground-truth sample (a), which is the target for the denoiser when given noisy image (b). With S for reduced and L for baseline. (c-f) are the cropped denoised outputs for input (b). The red square is a zoomed-in region. For higher noise levels, the denoising performance of Sequential is inferior to Integrated.

For joining the denoiser and classifier, we propose two models: (i) a Sequential model where the classifier is attached after the denoiser (Figure 2.i), and (ii) an Integrated model where the classifier is attached to the UNet encoder (Figure 2.ii). For Integrated, classification and denoising share the encoder, after which two branches are used, the decoder for denoising and another branch for classification.

The benefits of the Integrated model could come in threefold. First, using a shared encoder removes the need for a second large classifier, like in the Sequential method. Second, the decoder and classifier branches could run in parallel compared to running sequentially, which can result in lower latency. Thirdly, the decoder is only optimized for denoising as the optimization of the classifier does not influence it anymore. This should result in better image quality.

The models are trained using a weighted combination of the Cross-Entropy and Charbonnier loss [0.1 - 0.9], respectively weighted by 0.1 and 0.9. We report the metrics averaged over all 11 noise levels.

Exp. 1 Integrated vs. Sequential. Which joining method performs better for the baseline, and does the same hold when reducing its size? We compare the Sequential and Integrated models. In Table 3, we see that for both the baseline and reduced DC-Net models, the Integrated version performs significantly better at denoising, while the Sequential version performs better at classification. For higher noise levels, the Sequential models are not able to reconstruct the digit in detail, as visible in Figure 4.

Conclusion The integrated model has a slightly lower classification accuracy compared to the Sequential model. However, when aiming for improved human perception, it is still required for the human to see the content of the image. Therefore the Integrated model is more suitable.

4. Neural Architecture Search

We follow similar experimentation strategies as in the previous section. TF-NAS is used to construct a classifier, which we use as a basis for our denoiser and joint model.

Dataset & settings. NAS experiments are conducted on Imagenet [6], randomly cropped to 224x224 pixels. To reduce search and training time, 100 classes (Imagenet 100) from the original 1000 classes were chosen, as in [16]. In the experiments requiring noise, Gaussian noise is sampled uniformly with a continuous range of σ in $[0, 1]$.

The models are searched using SGD with momentum, 2E-2 LR with 90 epochs. After that, the found architecture is trained from scratch with 2E-1 LR for 250 epochs. All other settings are similar to [16]. The loss function form depends on the task of the experiment, smooth Cross-Entropy for classification ($\mathcal{L}_{\text{CE}}$), combined Charbonnier-SSIM for denoising ($\mathcal{L}_{\text{Char}}$,$\mathcal{L}_{\text{SSIM}}$), and a weighted combination for the joint model ($\mathcal{L}_{\text{Both}}$).

$$\mathcal{L}_{\text{Both}} = 0.1 \cdot \mathcal{L}_{\text{CE}} + 0.9 \cdot (0.8 \cdot \mathcal{L}_{\text{Char}} + 0.2 \cdot \mathcal{L}_{\text{SSIM}}) \quad (1)$$

Since our NAS method uses a latency look-up table constructed for our device, these experiments target a specific device, GeForce RTX 3090 GPU. Therefore latency is suitable for defining efficiency in the NAS experiments.

4.1. Classification: C-NAS

Experimental Setup. Since TF-NAS [16] learns β's to control the number of convolutional operators per stage, β's can reduce the model size. However, in the models proposed by [16], only 2 out of 24 stages are reduced by β. So the β's have little effect on the found architectures, yet they make the search space more complex. Therefore we propose a version of TF-NAS where the β's are removed so that all convolutional blocks are used.

The candidate operations in the search space of TF-NAS are MBConvs with 8 different configurations, see App. B. The configurations differ in kernel size, expansion rate, and in- or excluding a squeeze- and excitation layer (SE) [15].

The classification experiments are performed using data without noise, as the aim is to examine the NAS method, which is designed for clean images. We investigate key components of TF-NAS and try to improve its stability and classification performance.

Exp 1. Learned vs. Removed β. We conduct an experiment to study the effect of removing β on the search quality. The SE-layer is excluded from the candidate blocks, halving the search space to ensure the number of candidate operations does not cause search instability. We set a low target latency of 6 ms, as learning β should have a positive effect on small networks. For both the learned and removed settings, we run two searches, search 1 and 2.

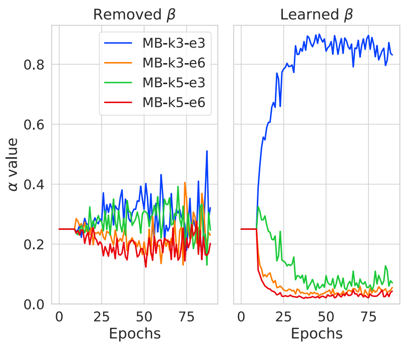

Figure 5. Stage-5:block-4's α values for Removed and Learned β. Search is more stable for Removed β.

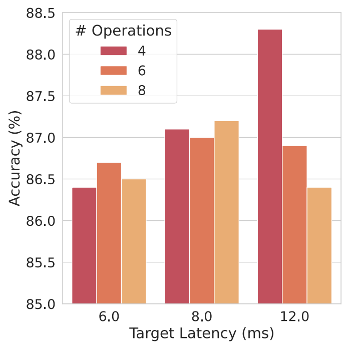

Figure 6. Acc for different search spaces, showed for different target latencies. Using fewer operations is most robust.

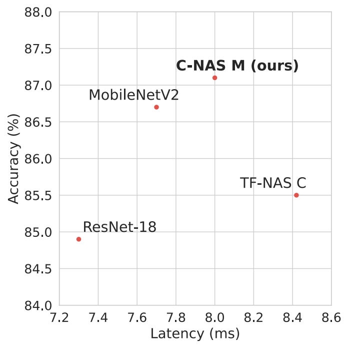

Figure 7. Comparing classifiers with similar latency. Our model classifies best, competing with MBNetV2

Figure 5 shows that when β is learned, the α's oscillate and therefore do not decide on an architecture. Whereas with Removed β, the search is stable. This stability reflects in the performance, as the average accuracy of the Removed β models is 86.3%, compared to 84.2% for Learned β. The separate results for each model are shown in Appendix C.

Exp 2. Number of operators in search space. Does reducing the number of operators during search positively influence the performance of the found models? We test this by comparing the performance of architectures searched with three different search space sizes, $\{4, 6, \text{or } 8\}$ operations, defined in App. B. For each of these search spaces, three different latency targets are used: $\{6, 8, \text{and } 12\}$ ms.

In Figure 6, we see that for lower target latencies, 6 and 8 ms, using fewer operations in the search space does not alter performance significantly. When targeting 12 ms latency, reducing the number of operations in the search space does show a significant improvement. Additionally, we find that when using the larger search spaces, the operators from the small search space are still preferred for lower latencies.

Exp 3. Compare with original TF-NAS. How do architectures found using our proposed changes to TF-NAS perform compared to models with similar latency? We compare our model, C-NAS M, with TF-NAS C, MobileNetV2, and ResNet-18. MobileNetV2 and our model have similar latency, architecture, and operator types. ResNet only differs in that it uses the Conv operator.

Figure 7 shows that the model found using our method (Figure 8.i) has lower latency yet higher accuracy than TF-NAS C as proposed in [16]. The model was searched with target latency 8.0. Therefore, it reached its target. Although ResNet-18 and MobileNetV2 run faster than our model, our classification accuracy is superior, especially when compared to ResNet-18, which only uses Convs.

Conclusion. By Removing β and reducing the number of operators used in the search, the search stability increases, and we find architectures that have better accuracy. An architecture found using our changes classifies better than a TF-NAS architecture with similar latency.

The comparison between our model and ResNet-18 shows that our search space is able to compete with widely accepted Conv-based classifiers. Moreover, our model performs on par with MobileNetV2, a manually designed classifier using MBConvs.

Model	UNet params: d	b	m	Lat. (ms) ↓	PSNR ↑	SSIM ↑
Reduced UNet	4	8	1.5	9.2	25.0	0.69
D-NAS S	-	-	-	9.45	**26.0**	**0.72**
UNet	5	64	2	116.5	**26.6**	**0.74**
D-NAS S upscaled	-	-	-	**109.8**	26.5	0.73

Table 4. Comparison of D-NAS and UNet variants for denoising. The rows are split into two latency ranges. D-NAS outperforms Reduced UNet. The larger variants perform similarly.

4.2. Denoising: D-NAS

Experimental setup. To construct a denoiser, D-NAS (Figure 8.ii), we use the first six stages of a found C-NAS classifier, which has four levels of resolution. Afterwards, we attach a UNet style decoder by using both a transposed convolution and two normal convolutions for each decoder level. Like UNet, we also add skip connections between the encoder and decoder layers. The decoder is not searched.

Exp 1. D-NAS vs UNet denoiser. Does our denoiser D-NAS perform similarly to the UNet denoisers? Reduced UNet (Section 3.2) is used, $\{d = 4, b = 8, c = 2, m = 1.5\}$, with a latency of 9.2 ms. We compare with D-NAS S, which is found by searching with a target latency of 9.2 ms. In addition, we test the standard UNet architecture. To compare with standard UNet, we increase the number of channels in D-NAS S to match the latency of both architectures.

Table 4 shows that D-NAS S outperforms Reduced UNet by 1.0 dB PSNR and 3% SSIM. The two large models perform similarly.

#	Model	Search		Lat. (ms) ↓	PSNR ↑	SSIM ↑	Acc. (%) ↑
		Images	Loss				
1	DC-NAS$_{\text{seq}}$ L	Clean	$\mathcal{L}_{\text{Cls}}$	18.3	25.0	0.69	76.0
	DC-NAS L	Clean	$\mathcal{L}_{\text{Cls}}$	**17.9**	**25.5**	**0.70**	76.0
2	DC-NAS$_{\text{clean}}$ M	Clean	$\mathcal{L}_{\text{Cls}}$	13.9	25.4	0.70	75.7
	DC-NAS$_{\text{noisy}}$ M	Noisy	$\mathcal{L}_{\text{Cls}}$	13.7	25.4	0.70	**76.0**
	DC-NAS$_{\text{noisy}}^{\mathcal{L}_{\text{Both}}}$ M	Noisy	$\mathcal{L}_{\text{Both}}$	13.8	25.4	0.70	75.5
3	C-NAS$_{\text{noisy}}$ M	Noisy	$\mathcal{L}_{\text{Cls}}$	7.9	-	-	75.5
4	DC-NAS$^{\text{mb}}$	Clean	$\mathcal{L}_{\text{Cls}}$	27.7	25.8	0.71	75.5
	DC-NAS$_{\text{1-op}}^{\text{mb}}$	Clean	$\mathcal{L}_{\text{Cls}}$	16.4	25.3	0.70	75.4
	DC-NAS$_{\text{3-lay}}^{\text{mb}}$	Clean	$\mathcal{L}_{\text{Cls}}$	22.1	25.4	0.70	75.1
5	DC-Net$_{\text{reduced}}$	-	-	10.0	24.5	0.68	61.9
	DC-Net$_{\text{reduced}}^{\text{tail}}$	-	-	10.5	24.6	0.69	68.6
	DC-NAS S	Noisy	$\mathcal{L}_{\text{Cls}}$	10.3	**25.4**	**0.70**	**74.3**

Table 5. DC-NAS experiments. 1: Sequential vs Integrated model. Similar latency and denoising performance, yet Integrated denoises better. 2: Different search strategies for DC-NAS. Searching on noisy images with only $\mathcal{L}_{\text{Cls}}$ performs best. 3: C-NAS$_{\text{noisy}}$ M vs DC-NAS$_{\text{noisy}}$ M. The Integrated model classifies better. 4: Using MBConvs in the DC-NAS$_{\text{noisy}}$ M decoder, and two downscaled versions. Original DC-NAS$_{\text{noisy}}$ is more efficient. 5: DC-NAS vs DC-Net. The NAS model outperforms the manually designed ones.

Conclusion. D-NAS outperforms our denoising baseline, UNet, for small models. Therefore D-NAS is a suitable denoising architecture, especially when kept small.

4.3. Joint Model: DC-NAS

Experimental setup. To construct the joint model, we use the Integrated and Sequential setup. The Integrated model, DC-NAS, is constructed similarly to D-NAS. As seen in Figure 8.iii, we connect the decoder after the first six stages of C-NAS but still use the remaining stages as classification branch. Whereas the Sequential model, DC-NAS$_{\text{seq}}$, is constructed by attaching C-NAS to the output of D-NAS, see Figure 8.iv. Therefore, the searched classifier is used twice in DC-NAS$_{\text{seq}}$, which increases its latency. To counter this, a smaller C-NAS model is used in both the encoder and classifier.

Exp 1. Compare Integrated vs. Sequential. We compare DC-NAS and DC-NAS$_{\text{seq}}$ models with similar latency. To get the same latency, C-NAS in DC-NAS$_{\text{seq}}$ L has low latency, only 6.7 ms. Whereas in DC-NAS L, C-NAS has a latency of 12 ms.

In Table 5:1, we see that both models have similar latency and the same classification accuracy, however, DC-NAS L improves denoising performance with 0.5 db PSNR and 1% SSIM.

Exp 2. Encoder search. C-NAS contains the searchable operations within DC-NAS. We test several search approaches: (i) using clean images, and (ii) using noisy images. For both approaches, we search the classifier using only classification loss. Resulting in models (i) DC-NAS$_{\text{clean}}$ M and (ii) DC-NAS$_{\text{noisy}}$ M. In addition, for approach (ii), we construct DC-NAS$_{\text{noisy}}^{\mathcal{L}_{\text{Both}}}$ M by searching using the combined denoising and classification loss. Therefore optimizing C-NAS for both tasks within DC-NAS$_{\text{noisy}}^{\mathcal{L}_{\text{Both}}}$. Regardless of the search method, the found models are trained using noisy images and the combined loss.

Table 5:2, shows that using noisy images during search improves classification accuracy, as DC-NAS$_{\text{clean}}$ M improves 0.3% acc compared to DC-NAS$_{\text{noisy}}$ M. Surprisingly, the denoising performance is the same. Using both the denoising and classification objective during the search, as in DC-NAS$_{\text{noisy}}^{\mathcal{L}_{\text{Cls}}}$, reduces the classification accuracy.

Exp 3. C-NAS vs DC-NAS. We are interested in the difference in noisy classification performance of C-NAS and DC-NAS. We remove the decoder from DC-NAS$_{\text{noisy}}$ to obtain C-NAS$_{\text{noisy}}$ and train it for classification.

We see that DC-NAS$_{\text{noisy}}$, improves classification accuracy by 0.5% compared to C-NAS$_{\text{noisy}}$, in Table 5:2-3.

Exp 4. Decoder tuning. All models found in Experiment 2, have similar denoising performance. These models have the same latency but differ only in the operators that are used in the encoder. We test if the denoising performance is influenced by adjusting the operators in the decoder while retaining the latency. DC-NAS$_{\text{clean}}$ M is used as a basis. We construct three alternatives. (i) DC-NAS$^{\text{mb}}$, for which the convolutional operators in the decoder are replaced with MBConvs (MB-k3-e3), which significantly increases the latency of the model. To account for this, we also test with (ii) DC-NAS$_{\text{1-op}}^{\text{mb}}$, where 1 instead of 2 MBConvs are used per layer and (iii) DC-NAS$_{\text{3-lay}}^{\text{mb}}$ where we reduce the number of decoder layers by one. Method (ii) and (iii) relate to scaling c and d in Section 3.2, where scaling the number of channels (b), was found more effective. Scaling b is not considered here as this would require altering the encoder too.

In Table 5:4, we see that DC-NAS$^{\text{mb}}$ compared to DC-NAS$_{\text{clean}}$ M improves the denoising performance. However, at the cost of 13.8 ms latency increase, only caused by the MB decoder. When reducing the complexity of the MB decoder with DC-NAS$_{\text{1-op}}^{\text{mb}}$ and DC-NAS$_{\text{3-lay}}^{\text{mb}}$, the denoising performance reduces to the original level again, but the latency is still higher than for DC-NAS$_{\text{clean}}$ M.

Exp 5. DC-Net vs DC-NAS How does our model, constructed by search, compare to the model we manually constructed? DC-NAS S is searched on noisy data with a target latency set to the actual latency of DC-Net Reduced, from Section 3.3. Since the classification branch of DC-Net is designed for the simpler synthetic dataset, we also test with DC-Net$^{\text{tail}}$, which uses the same classification branch as DC-NAS S.

Table 5:5, shows that DC-NAS S outperforms both DC-Net models by at least 0.8 dB PSNR, 1% SSIM, and 5.7% accuracy. We display the denoising results of DC-NAS S

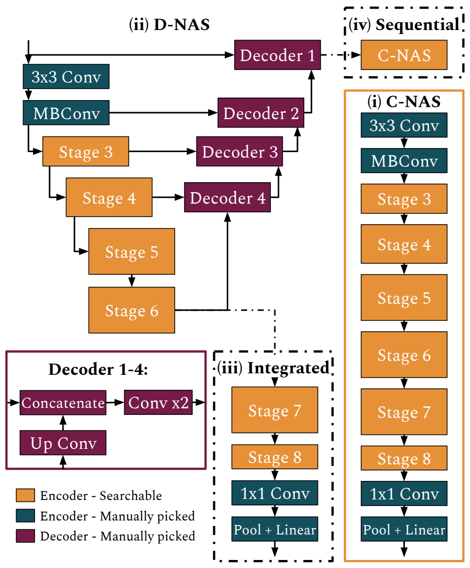

Figure 8. C-NAS and D-NAS architecture. Attach (iii) for DC-NAS and (iv) for DC-NAS$_{\text{seq}}$. Searchable stages consist of a maximum of four MBConvs.

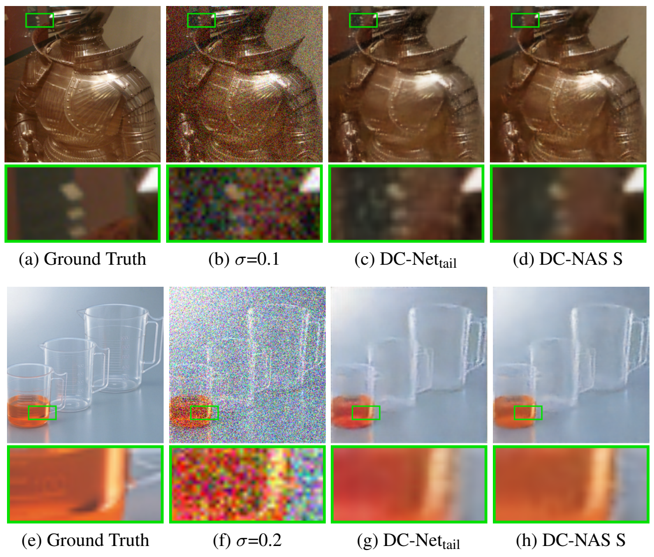

Figure 9. Denoising performance of DC-Net$_{\text{tail}}$ and DC-NAS S. Left to right: clean image, noisy variant, and the denoiser output. Comparing (c) and (d), we see better performance on a smooth plane and slightly sharper edges for (c). With (g) and (h), we see observe a better color reconstruction for (h).

and DC-Net$^{\text{tail}}$ in Figure 9. We observe better denoising on smooth planes, sharper edges and better color reconstruction for DC-NAS S.

Conclusion. We have seen that the Integrated combining method outperforms its Sequential counterpart in denoising. To construct the integrated model, we find that searching for a classifier on noisy data, without taking the denoising objective into account results in the best classification performance. Surprisingly, the search method does not influence the denoising performance. Furthermore, replacing the convolutional blocks in the decoder with MBConvs and then scaling them down does not benefit denoising efficiency either. However, the NAS denoising experiments demonstrate that our denoising setup is competitive and gains performance when scaled significantly. Since up-scaling is not of interest for our models and tuning the decoder operators does not improve performance, our method is focused on searching for only the encoder of the integrated model. The models found by this approach, outperform our manually designed models with similar latency.

5. Limitations & Conclusion

One limitation of our NAS method is its inability to alter the decoder. It is designed this way as manually altering the decoder does not improve efficiency. However, when targeting a significantly different latency, a change in denoising architecture could be optimal. Applying model scaling to the found models is of interest, similar to the EfficientNets [31, 32].

Another limitation is the fixation of β in our NAS method. Although this improved the stability of search and network performance, learning β while retaining a stable search would be preferred. As this would introduce more possibilities in the search space for optimizing efficiency.

In addition, the Integrated models already outperform the Sequential alternatives, but latency could be optimized further for Integrated models by running the denoising and classification branches in parallel.

To conclude, we show that using efficient operators and scaling methods proposed in previous work are relevant for denoising and noisy classification. In addition, we present the integrated model to join the two tasks efficiently. We analyze how the performance of the Integrated model compares to the Sequential model. This shows that the Integrated design is more suitable across various latencies. To simplify the design process of the joint model when targeting a latency, we present a NAS method. We alter an existing NAS method to improve the stability and performance of the search. This method searches a classifier. Using the searched classifier as a basis, we build the Integrated model. We demonstrate that the Integrated model built using our NAS method outperforms the manually constructed model.

References

[1] Han Cai, Ligeng Zhu, and Song Han. Proxylessnas: Direct neural architecture search on target task and hardware. *CoRR*, abs/1812.00332, 2018. 2

[2] P. Charbonnier, L. Blanc-Feraud, G. Aubert, and M. Barlaud. Two deterministic half-quadratic regularization algorithms for computed imaging. In *Proceedings of 1st International Conference on Image Processing*, volume 2, pages 168–172 vol.2, 1994. 4

[3] Anda Cheng, Jiaxing Wang, Xi Sheryl Zhang, Qiang Chen, Peisong Wang, and Jian Cheng. DPNAS: neural architecture search for deep learning with differential privacy. *CoRR*, abs/2110.08557, 2021. 2

[4] Xiangxiang Chu, Tianbao Zhou, Bo Zhang, and Jixiang Li. Fair DARTS: eliminating unfair advantages in differentiable architecture search. *CoRR*, abs/1911.12126, 2019. 2

[5] Kostadin Dabov, Alessandro Foi, Vladimir Katkovnik, and Karen Egiazarian. Image denoising by sparse 3-d transform-domain collaborative filtering. *IEEE Transactions on Image Processing*, 16(8):2080–2095, 2007. 1, 2

[6] Jia Deng, Wei Dong, Richard Socher, Li-Jia Li, Kai Li, and Li Fei-Fei. Imagenet: A large-scale hierarchical image database. In *2009 IEEE conference on computer vision and pattern recognition*, pages 248–255. Ieee, 2009. 5

[7] Li Deng. The mnist database of handwritten digit images for machine learning research. *IEEE Signal Processing Magazine*, 29(6):141–142, 2012. 3

[8] Bappaditya Dey, Sandip Halder, Kasem Khalil, Gian Lorusso, Joren Severi, Philippe Leray, and Magdy A. Bayoumi. SEM image denoising with unsupervised machine learning for better defect inspection and metrology. In Ofer Adan and John C. Robinson, editors, *Metrology, Inspection, and Process Control for Semiconductor Manufacturing XXXV*, volume 11611, page 1161115. International Society for Optics and Photonics, SPIE, 2021. 1

[9] Chi-Mao Fan, Tsung-Jung Liu, and Kuan-Hsien Liu. SUNet: Swin transformer UNet for image denoising. In *2022 IEEE International Symposium on Circuits and Systems (ISCAS)*. IEEE, may 2022. 2

[10] Shuhang Gu, Yawei Li, Luc Van Gool, and Radu Timofte. Self-guided network for fast image denoising. In *Proceedings of the IEEE/CVF International Conference on Computer Vision (ICCV)*, October 2019. 1

[11] Shuhang Gu, Lei Zhang, Wangmeng Zuo, and Xiangchu Feng. Weighted nuclear norm minimization with application to image denoising. In *2014 IEEE Conference on Computer Vision and Pattern Recognition*, pages 2862–2869, 2014. 1, 2

[12] Javier Gurrola-Ramos, Oscar Dalmau, and Teresa E. Alarcón. A residual dense u-net neural network for image denoising. *IEEE Access*, 9:31742–31754, 2021. 1, 2

[13] Andrew Howard, Mark Sandler, Grace Chu, Liang-Chieh Chen, Bo Chen, Mingxing Tan, Weijun Wang, Yukun Zhu, Ruoming Pang, Vijay Vasudevan, Quoc V. Le, and Hartwig Adam. Searching for mobilenetv3. *CoRR*, abs/1905.02244, 2019. 2

[14] Andrew G. Howard, Menglong Zhu, Bo Chen, Dmitry Kalenichenko, Weijun Wang, Tobias Weyand, Marco Andreetto, and Hartwig Adam. Mobilenets: Efficient convolutional neural networks for mobile vision applications. *CoRR*, abs/1704.04861, 2017. 2

[15] Jie Hu, Li Shen, and Gang Sun. Squeeze-and-excitation networks. *CoRR*, abs/1709.01507, 2017. 5

[16] Yibo Hu, Xiang Wu, and Ran He. TF-NAS: rethinking three search freedoms of latency-constrained differentiable neural architecture search. *CoRR*, abs/2008.05314, 2020. 1, 2, 5, 6, 11

[17] Ding Liu, Bihan Wen, Jianbo Jiao, Xianming Liu, Zhangyang Wang, and Thomas S. Huang. Connecting image denoising and high-level vision tasks via deep learning. *CoRR*, abs/1809.01826, 2018. 1, 2

[18] Hanxiao Liu, Karen Simonyan, and Yiming Yang. DARTS: differentiable architecture search. *CoRR*, abs/1806.09055, 2018. 2

[19] Pengju Liu, Hongzhi Zhang, Kai Zhang, Liang Lin, and Wangmeng Zuo. Multi-level wavelet-cnn for image restoration. *CoRR*, abs/1805.07071, 2018. 2

[20] Damian J. Matuszewski and Ida-Maria Sintorn. Reducing the u-net size for practical scenarios: Virus recognition in electron microscopy images. *Computer Methods and Programs in Biomedicine*, 178:31–39, 2019. 1, 3

[21] Sameera V. Mohd Sagheer and Sudhish N. George. A review on medical image denoising algorithms. *Biomedical Signal Processing and Control*, 61:102036, 2020. 1

[22] Marcin Możejko, Tomasz Latkowski, Łukasz Treszczotko, Michał Szafraniuk, and Krzysztof Trojanowski. Superkernel neural architecture search for image denoising, 2020. 2

[23] James O'Neill. An overview of neural network compression. *CoRR*, abs/2006.03669, 2020. 2

[24] Bumjun Park, Songhyun Yu, and Jechang Jeong. Densely connected hierarchical network for image denoising. In *2019 IEEE/CVF Conference on Computer Vision and Pattern Recognition Workshops (CVPRW)*, pages 2104–2113, 2019. 2

[25] Hieu Pham, Melody Y. Guan, Barret Zoph, Quoc V. Le, and Jeff Dean. Efficient neural architecture search via parameter sharing. *CoRR*, abs/1802.03268, 2018. 2

[26] Olaf Ronneberger, Philipp Fischer, and Thomas Brox. U-net: Convolutional networks for biomedical image segmentation. *CoRR*, abs/1505.04597, 2015. 2

[27] Mark Sandler, Andrew G. Howard, Menglong Zhu, Andrey Zhmoginov, and Liang-Chieh Chen. Inverted residuals and linear bottlenecks: Mobile networks for classification, detection and segmentation. *CoRR*, abs/1801.04381, 2018. 1, 2, 3

[28] Karen Simonyan and Andrew Zisserman. Very deep convolutional networks for large-scale image recognition, 2015. 2

[29] Prabhishek Singh and Achyut Shankar. A novel optical image denoising technique using convolutional neural network and anisotropic diffusion for real-time surveillance applications. *Journal of Real-Time Image Processing*, 18(5):1711–1728, Oct 2021. 1

[30] Mingxing Tan, Bo Chen, Ruoming Pang, Vijay Vasudevan, and Quoc V. Le. Mnasnet: Platform-aware neural architecture search for mobile. *CoRR*, abs/1807.11626, 2018. 2

[31] Mingxing Tan and Quoc V. Le. Efficientnet: Rethinking model scaling for convolutional neural networks. *CoRR*, abs/1905.11946, 2019. 1, 2, 3, 8

[32] Mingxing Tan and Quoc V. Le. Efficientnetv2: Smaller models and faster training. *CoRR*, abs/2104.00298, 2021. 2, 3, 8, 11

[33] Zhou Wang, A.C. Bovik, H.R. Sheikh, and E.P. Simoncelli. Image quality assessment: from error visibility to structural similarity. *IEEE Transactions on Image Processing*, 13(4):600–612, 2004. 3

[34] Zhendong Wang, Xiaodong Cun, Jianmin Bao, and Jianzhuang Liu. Uformer: A general u-shaped transformer for image restoration. *CoRR*, abs/2106.03106, 2021. 2

[35] Bichen Wu, Xiaoliang Dai, Peizhao Zhang, Yanghan Wang, Fei Sun, Yiming Wu, Yuandong Tian, Peter Vajda, Yangqing Jia, and Kurt Keutzer. Fbnet: Hardware-aware efficient convnet design via differentiable neural architecture search. *CoRR*, abs/1812.03443, 2018. 2, 11

[36] Jiqing Wu, Radu Timofte, Zhiwu Huang, and Luc Van Gool. On the relation between color image denoising and classification. *arXiv preprint arXiv:1704.01372*, 2017. 2

[37] Yuxin Wu and Kaiming He. Group normalization. *CoRR*, abs/1803.08494, 2018. 3

[38] Sirui Xie, Hehui Zheng, Chunxiao Liu, and Liang Lin. SNAS: stochastic neural architecture search. *CoRR*, abs/1812.09926, 2018. 2

[39] Peng Ye, Baopu Li, Yikang Li, Tao Chen, Jiayuan Fan, and Wanli Ouyang. β-darts: Beta-decay regularization for differentiable architecture search, 2022. 2

[40] Haokui Zhang, Ying Li, Hao Chen, and Chunhua Shen. IR-NAS: neural architecture search for image restoration. *CoRR*, abs/1909.08228, 2019. 2

[41] Kai Zhang, Wangmeng Zuo, Yunjin Chen, Deyu Meng, and Lei Zhang. Beyond a gaussian denoiser: Residual learning of deep CNN for image denoising. *CoRR*, abs/1608.03981, 2016. 1, 2

[42] Kai Zhang, Wangmeng Zuo, and Lei Zhang. FFDNet: Toward a fast and flexible solution for CNN-based image denoising. *IEEE Transactions on Image Processing*, 27(9):4608–4622, sep 2018. 1

[43] Xiangyu Zhang, Xinyu Zhou, Mengxiao Lin, and Jian Sun. Shufflenet: An extremely efficient convolutional neural network for mobile devices. *CoRR*, abs/1707.01083, 2017. 2

A. Efficient Classification: Additional results

In Section 3.1, we compare the performance of MBConv operations with normal convolutions. We present the results for scaling the MBConv and Conv models.

Exp. 2: MBConv width & expansion rate scaling. Since MBConv layers can be used to improve efficiency, we question how to further reduce the MB model's FLOP size. We compare two options: (i) reducing the expansion rate and (ii) scaling the width of the network. We take MB4-L as starting model, as this is our best and largest model.

From the MB models with size S in Table 6, MB1-S performs the worst. It only has a reduced expansion rate from 4 to 1. MB4-S, which is obtained by scaling the width of MB-L, increases classification performance by only 0.4%. However, when slightly reducing MB4-L's width and expansion rate, we derive MB2.5-S, which reaches 58.4% accuracy, significantly outperforming both other S-sized MB models. So the combination of the two methods is most effective.

Exp. 3: Conv width scaling. In this experiment, we compare the width scaling of the Conv-L model. Table 6 shows that all S-sized MB models outperform Conv-S, MB2.5-S even by 3.0%. MB2.5-M also outperforms Conv-M, by 2.7%. Therefore, scaling is more efficient for the MB models than the Conv models when optimizing for FLOPs.

Exp.	Model	Size	Exp. rate	FLOPs (K) $\downarrow$	Lat. (ms) $\downarrow$	Acc (%) $\uparrow$
1-3	Conv-L	L	-	447	0.336	63.2
	MB1-S	S	1	177	0.300	56.2
	MB2.5-M	M	2.5	350	0.384	64.1
	MB4-L	L	4	424	0.468	64.9
2-3	MB2.5-S	S	2.5	178	0.390	58.4
	MB4-S	S	4	188	0.403	56.6
3	Conv-S	S	-	163	0.281	55.4
	Conv-M	M	-	345	0.317	61.4

Table 6. Classification baseline and reduced models, designed for three different FLOP targets: $\{S, M, L\}$, to compare scaling methods: expansion rate and model width. Each section of rows is used by the experiments from Sec. 3.1 defined in the *Exp.* column. MB models scale down more efficiently than normal Conv models.

B. Search space

In Section 4.1, different variations of the TF-NAS search space are used [16]. Table 7 displays the candidate operations and for which search space size they are used. The search space with 4 operators is constructed using the MB-Convs without SE-layer, as this is most common in recent NAS methods [32, 35]. For the 6-operator search space, we add the possibility of using an SE layer on the operators where the kernel size is three and the expansion rate is three or six. We use the two smallest operators as they can be used for smaller target latencies too. The search space with 8 operators simply uses all combinations.

Name	Kernel	Expansion rate	SE-layer	4	6	8
MB-k3-e3	3	3	-	✓	✓	✓
MB-k3-e6	3	6	-	✓	✓	✓
MB-k5-e3	5	3	-	✓	✓	✓
MB-k5-e6	5	6	-	✓	✓	✓
MB-k3-e3-se	3	3	✓	-	✓	✓
MB-k3-e6-se	3	6	✓	-	✓	✓
MB-k5-e3-se	5	3	✓	-	-	✓
MB-k5-e6-se	5	6	✓	-	-	✓

Table 7. Overview of the candidate blocks for the different search space sizes {4, 6, 8}. MBConv operators are used with different kernel sizes *k*, expansion rate *e* and in- or excluding the squeeze-and excitation-layer.

C. Learned vs. Removed β: Additional results

In Experiment 1 of Section 4.1, we test the influence of removing β from the search approach. The models with Removed β significantly outperform the models with Learned β in accuracy. Besides, the found models are more similar for Removed than Fixed, Removed β differs only 0.04ms and 0.2% accuracy, while Learned β differs 0.57ms and 1.4% accuracy. This indicates that the search for Removed is more stable.

Type	Search id	LAT (ms) ↓	Acc (%) ↑
Removed β	1	5.85	**86.2**
	2	5.81	**86.4**
Learned β	1	5.04	84.9
	2	4.47	83.5

Table 8. Compares four searched models with target latency 6 ms. Trained on clean images. Two models are searched without β and the other two using learned β. Removed outperforms learned β.